

An Evolved Orthogonal Enzyme/Cofactor Pair

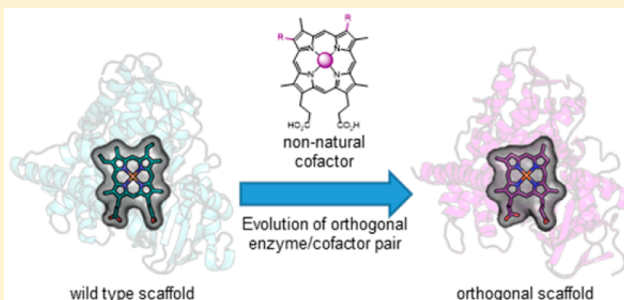
Evan W. Reynolds,[†] Matthew W. McHenry,[†] Fabien Cannac,[†] Joshua G. Gober,[†] Christopher D. Snow,[‡] and Eric M. Brustad^{*,†}

[†]Department of Chemistry, University of North Carolina—Chapel Hill, 125 South Road, CB 3290, Chapel Hill, North Carolina 27599, United States

[‡]Department of Chemical and Biological Engineering, Colorado State University, Fort Collins, Colorado 80523, United States

S Supporting Information

ABSTRACT: We introduce a strategy that expands the functionality of hemoproteins through orthogonal enzyme/heme pairs. By exploiting the ability of a natural heme transport protein, Chua, to promiscuously import heme derivatives, we have evolved a cytochrome P450 (P450_{BM3}) that selectively incorporates a nonproteinogenic cofactor, iron deuteroporphyrin IX (Fe-DPIX), even in the presence of endogenous heme. Crystal structures show that selectivity gains are due to mutations that introduce steric clash with the heme vinyl groups while providing a complementary binding surface for the smaller Fe-DPIX cofactor. Furthermore, the evolved orthogonal enzyme/cofactor pair is active in non-natural carbenoid-mediated olefin cyclopropanation. This methodology for the generation of orthogonal enzyme/cofactor pairs promises to expand cofactor diversity in artificial metalloenzymes.



INTRODUCTION

The introduction of non-natural metallocofactors into proteins is a powerful means of expanding protein chemical functionality and has been utilized to probe protein structure and function,^{1–3} to create novel biosensors,^{4–6} and to promote non-natural biocatalysis.^{7–9} Several methods have been developed for the *in vitro* immobilization of artificial metallocofactors within proteins,⁷ including the supramolecular anchoring of biotinylated metal complexes into streptavidin^{10,11} and the covalent anchoring of metal complexes via strain-promoted azide–alkyne cycloadditions.¹² Others have sought to repurpose existing cofactor sites within proteins. In particular, hemoproteins have been the target of a variety of cofactor substitution protocols.^{3,13–15} Such substitution is commonly accomplished via acid denaturation and subsequent organic extraction to remove heme, followed by reconstitution of the protein in the presence of a non-natural metal cofactor (e.g., metallo-salens and -porphyrins, etc.).^{3,13,14} These *in vitro* methods generate new metal centers that can be further tuned through mutagenesis;^{16–18} however, they are labor-intensive and often result in low reconstituted protein yields.

To overcome challenges associated with *in vitro* cofactor replacement, two complementary strategies have been developed to permit the cellular uptake and incorporation of artificial heme-like cofactors into proteins. Overexpression of a native heme-transport channel, Chua, has enabled the import of metal-swapped protoporphyrin IX derivatives in *Escherichia coli*.^{5,19} This approach, however, is limited by competition between the synthetic cofactor and native heme, which is the preferred prosthetic group of wild type hemoproteins.

Accordingly, metal substitution via Chua is carried out in iron-deficient minimal media to minimize heme biosynthesis, and even in these cases a small amount of heme contamination (~2–5%) is observed.⁵ Heme-substituted proteins have been produced with high purity (>99%) using a specialized strain of *E. coli* that combines a knockout in heme biosynthesis and an uncharacterized mutation that promotes membrane permeability to synthetic hemes, permitting incorporation of a variety of heme derivatives with modifications to both the metal center and/or the porphyrin scaffold.^{4,6,20,21} Nevertheless, this method necessitates anaerobic conditions for growth, which limits yield and throughput.²⁰

We introduce a new approach for the construction of non-natural metallocofactor proteins via the evolution of orthogonal enzyme/heme pairs (Figure 1A). Orthogonal enzyme/heme pairs comprise a non-natural heme-like cofactor and a complementary heme-binding protein that selectively interact independent of the cell's native heme machinery. This strategy of generating orthogonal enzyme/cofactor pairs has been applied to other systems, including nicotinamide adenine dinucleotide-^{22,23} and S-adenosyl methionine (SAM)-utilizing enzymes.²⁴

Here, we demonstrate the *in vivo*, selective incorporation of a nonproteinogenic metalloporphyrin, iron deuteroporphyrin IX (Fe-DPIX), in place of heme in a model bacterial cytochrome P450 from *Bacillus megaterium* (P450_{BM3}).²⁵ Through directed evolution²⁶ of the P450_{BM3} heme-binding pocket, a P450

Received: June 7, 2016

Published: August 30, 2016

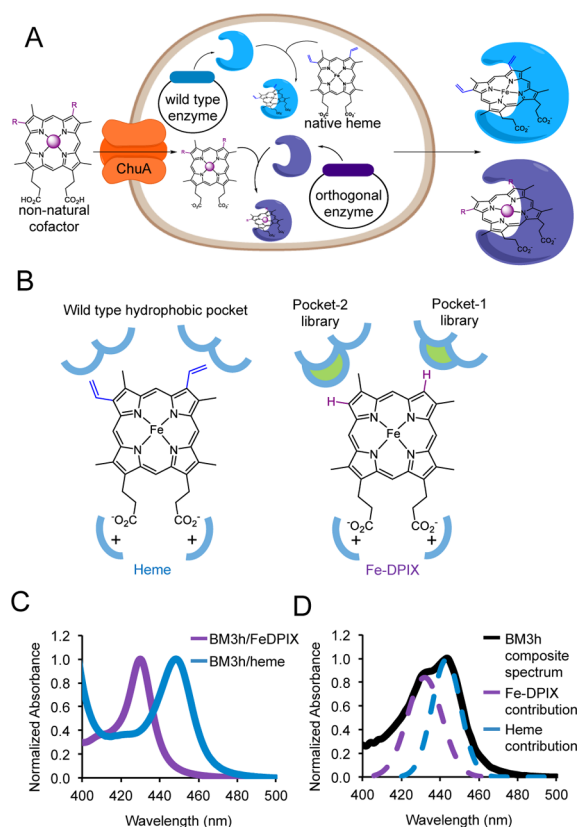


Figure 1. Orthogonal enzyme/heme pairs: concept and screening. (A) Heme transport channel, ChuA (orange), enables cellular import of non-natural heme derivatives (purple) that selectively bind to orthogonal protein scaffolds (purple) without cross-talk with endogenous heme and hemoproteins (black and blue, respectively). (B) Replacing the vinyl groups of heme (blue) with hydrogens (purple) in Fe-DPIX creates a cavity that may be filled by amino acid mutations (green semicircles) located within adjacent hydrophobic pockets-1 and -2. (C) Absorbance spectra of purified ferrous CO-bound BM3h in complex with Fe-DPIX (purple) or heme (blue). (D) Absorbance spectrum (solid black line) of ferrous CO-bound BM3h expressed in rich media supplemented with Fe-DPIX and heme. The relative contribution of the Fe-DPIX- and heme-bound enzyme to the composite spectrum have been approximated by a Gaussian fit centered at 434 nm (purple dotted line) and 450 nm (blue dotted line), respectively.

variant was isolated that selectively binds Fe-DPIX with >99% purity in minimal media, and 95% enrichment of Fe-DPIX in nutrient-rich environments under which cells produce endogenous heme. Crystal structures of variants along the evolutionary trajectory reveal an iterative reduction in size of the cofactor-binding pocket, resulting in exclusion of heme from the enzyme while accommodating Fe-DPIX. Furthermore, the orthogonal enzyme/cofactor pair shows non-natural catalytic activity in carbenoid-mediated cyclopropanation, highlighting the potential of this system to expand biocatalytic reaction space. We anticipate that orthogonal enzyme/cofactor pairs may provide a general strategy for increasing cofactor diversity and expanding protein chemical functionality in cells.

RESULTS AND DISCUSSION

BM3h/Fe-DPIX as a Model Orthogonal Enzyme/Cofactor Pair. To demonstrate the feasibility of generating orthogonal enzyme/cofactor pairs, cytochrome P450_{BM3} was

chosen as a target scaffold. P450_{BM3} is a soluble, self-sufficient (i.e., consists of fused heme and P450-reductase domains) monooxygenase that has been extensively studied.²⁵ P450_{BM3} has been engineered for a number of applications including altered substrate scope,²⁷ increased thermostability,²⁸ and tolerance to organic solvent,²⁹ attesting to the flexibility of this scaffold to accommodate mutations. Furthermore, the isolated heme domain of P450_{BM3} (BM3h) has been the subject of several cofactor substitution studies.^{5,30,31}

We initiated cofactor replacement efforts by focusing on a commercially available metalloporphyrin, Fe-DPIX, which differs from native heme by the deletion of the two exocyclic vinyl moieties (Figure 1B). We hypothesized that the remaining heme-like features of Fe-DPIX, including iron–metal center, aromatic tetrapyrrole scaffold, and carboxylate side chains, would promote promiscuous uptake by ChuA and provide conserved motifs to facilitate binding within the BM3h heme pocket. Concomitantly, the “holes” created by deletion of the vinyl groups would serve as discriminating handles to accommodate mutations that enrich binding of Fe-DPIX in lieu of heme (Figure 1B). Similar “bump-hole” strategies have been applied to a variety of different systems, including design of ATP mimetics that selectively interact with engineered protein kinases,³² and SAM analogues for engineered histone methyltransferases,²⁴ among others.^{33,34}

In Vivo Incorporation of Fe-DPIX into Wild Type BM3h. To test for cellular uptake of Fe-DPIX and its accommodation within BM3h, ChuA and BM3h were coexpressed in *E. coli* grown in iron-deficient minimal media (to restrict cellular heme production) that was supplemented with 10 μ M Fe-DPIX. Reduced CO-bound BM3h/Fe-DPIX shows a distinctive Soret band at 434 nm (Figure 1C) that is blue-shifted from native BM3h, which displays a Soret peak at 450 nm characteristic of cytochrome P450s.³⁵ The hypsochromic shift observed for the Fe-DPIX Soret band is consistent with decreased conjugation around the porphyrin ring resulting from removal of the vinyl groups. BM3h/Fe-DPIX production was dependent on ChuA overexpression (Supporting Information, Figure S1). This observation suggests that ChuA can provide broadened cellular access to metallocofactors that contain at least small modifications to the protoporphyrin IX scaffold.

Fe-DPIX and heme content in wild type BM3h preparations were quantified using a customized high-performance liquid chromatography (HPLC) assay (Figure S2, Table S4). Under reverse-phase conditions, BM3h denatures, releasing both cofactors and allowing for separation and comparison against calibration curves constructed for each cofactor.

Using this assay, the yield of Fe-DPIX-containing protein expressed in minimal media was determined to be \sim 30 mg/L. Even under these stringent conditions, small levels of heme contamination (\sim 2%) were observed (yields and mol % Fe-DPIX are reported in Table 1). In contrast, BM3h expressed in rich media (i.e., in the presence of endogenous heme) supplemented with ectopic Fe-DPIX yields a 62.7:37.3 mixture of Fe-DPIX and heme-containing protein, respectively (Table 1).

An Absorbance-Based Assay for Cofactor Enrichment.

The 16 nm Soret band shift observed in BM3h/Fe-DPIX provides a convenient spectroscopic handle to distinguish Fe-DPIX and heme content in complex mixtures, which can be used to screen for mutations that lead to changes in cofactor selectivity. When expressed in rich media (Terrific Broth, TB) supplemented with 10 μ M heme and 10 μ M Fe-DPIX, a

Table 1. Characterization of BM3h Variants, Including Mutations, Selectivity in Rich Media and Minimal Media, Thermostability, and Yield^a

variant	mutations	mol % ^b (TB media)			mol % ^b (M9 media)			T ₅₀ (°C)		M9 yield (mg/L) ^c
		Fe-DPIX	heme	error ^a	Fe-DPIX	heme	error ^a	Fe-DPIX	heme	Fe-DPIX
WT	none	62.7	37.3	4.5	98.8	1.2	1.5	50.4 ± 0.1	55.5 ± 1.5	28 ± 8
WIV	T269V, L272W, L322I	71.4	28.6	9.5	99.5	0.5	0.03	51.2 ± 0.2	52.7 ± 0.2	29 ± 10
WIVS	T269V, L272W, L322I, A406S	74.3	25.7	3.8	98.3	1.7	1.5	49.4 ± 0.9	49.7 ± 0.8	40 ± 5
WIVS-FM	G265F, T269V, L272W, L322I, F405M, A406S	95.0 ^c	5.0 ^c	1.8 ^c	>99.9 ^d	n.d. ^d	n/a ^d	47.1 ± 1.1	n.d.	15 ± 5
FM	G265F, F405M	77.4	22.6	6.0	94.5	5.5	4.4	48.3 ± 0.2	51.0 ± 0.2	10 ± 4
S-FM	G265F, F405M, A406S	89.5	10.5	4.0	99.7	0.3	0.3	49.4 ± 2.7	n.d.	14 ± 1
WIV-FM	G265F, T269V, L272W, L322I, F405M	89.6	10.4	2.3	99.9	0.1	0.1	51.1 ± 0.5	50.1 ± 0.1	34 ± 12
WIVS-FM-IV	L52I, G265F, T269V, L272W, L322I, I366V, F405M, A406S	84.6	15.4	2.0	97.6	2.4	0.7	51.4 ± 0.4	50.1 ± 0.1	31 ± 2

^aAll values reported are the average and standard deviations from three independent experiments unless otherwise noted. ^bDetermined by HPLC analysis of purified proteins from expressions in the denoted media. ^cAverage and standard deviation from eight independent experiments. ^dAverage and standard deviation from seven independent experiments. ^eYields were determined via HPLC analysis or from ferrous CO-bound difference spectra, using $\epsilon_{430\text{ nm}} = 130\text{ mM}^{-1}\text{ cm}^{-1}$.

mixture of Fe-DPIX- and heme-bound BM3h is observed. A Matlab script was developed to fit CO-bound absorbance spectra as Gaussian functions centered at 434 and 450 nm (Figure 1D) to approximate the ratio of incorporation of Fe-DPIX with respect to heme for a particular variant. This assay is readily adaptable to high throughput analysis of BM3h-hemocompositions in lysate and on a multiwell format.

Evolution of an Fe-DPIX-Specific Protein. Analysis of BM3h crystal structures^{36,37} reveals two distinct binding pockets, which we denote as pocket-1 and pocket-2, that accommodate the vinyl groups of heme (Figure 2A). These pockets are composed primarily of hydrophobic amino acids that provide a complementary surface to accommodate the porphyrin scaffold. We hypothesized that mutations that fill the cavities imparted by removal of the heme vinyl groups may provide productive binding interactions for the selective discrimination of Fe-DPIX while concomitantly introducing steric clashes that prevent heme recognition (Figure 1B).

We initiated our screening efforts by investigating the ability of mutations to replace the pocket-1 vinyl moiety. Since protein/Fe-DPIX interactions in this pocket are likely to involve hydrophobic and van der Waals contacts, we created a limited-diversity library randomizing active site residues to 10 hydrophobic or aromatic amino acids—Gly, Ala, Val, Leu, Ile, Met, His, Phe, Tyr, and Trp—at each position, allowing us to restrict library size and in parallel maximize the number of residues available for mutation. Similar limited-diversity strategies have been used to improve the likelihood of identifying hits while reducing screening effort.³⁸

Mutations were focused at residues T269, L272, and L322 (Figure 2A, left) providing a library diversity of 10³ possible variants. From this library, 1000 transformants were screened in rich media, as described above. Three variants were isolated that showed improvements in Fe-DPIX binding (Figure 2B and Table S2). Notably, all three variants converged on similar mutations including a Trp and Ile mutation at positions 272 and 322, respectively, and a small hydrophobic amino acid at position 269. The best variant, BM3h-T269V/L272W/L322I (denoted WIV), was chosen for further optimization. A CO-bound absorbance spectrum showing the increase in Fe-DPIX incorporation by WIV with respect to wild type BM3h is shown in Figure 2B. To achieve further improvements in pocket-1 Fe-DPIX selectivity, we next constructed a site-saturation library

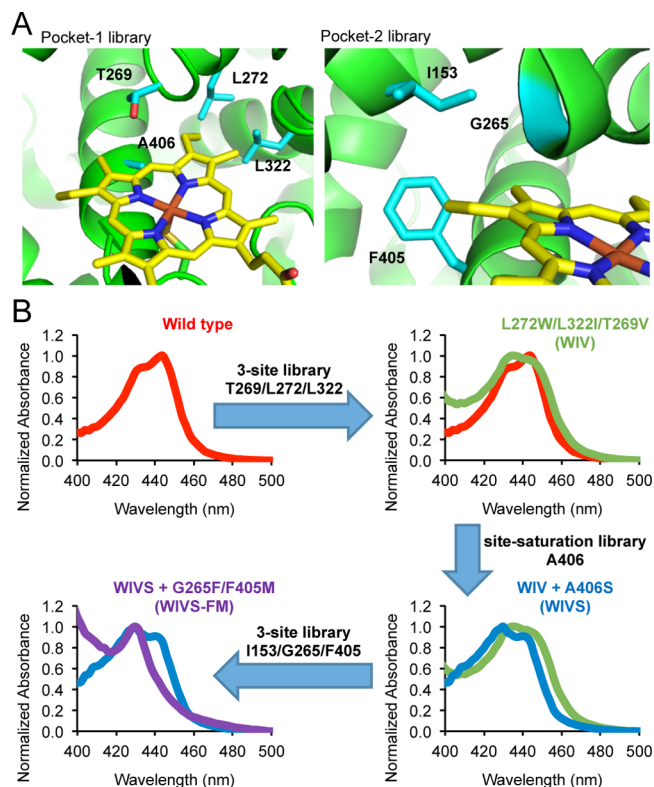


Figure 2. Engineering BM3h for selective recognition of Fe-DPIX. (A) Crystal structure of wild type BM3h (green, PDB: 2IJ2³⁶) highlighting side chains targeted for mutation (blue) as well as the heme cofactor (yellow). (B) Absorbance spectra for ferrous-CO bound BM3h variants along the evolutionary trajectory: wild type (red), WIV (green), WIVS (blue), and WIVS-FM (purple).

(all 20 possible amino acid substitutions) focused at position A406 using WIV as a template. An additional mutation WIV-A406S (WIVS) was identified that improved Fe-DPIX incorporation when compared to the WIV parent (Figure 2B). Introduction of the A406S mutation resulted in a slight blue-shift of the Soret band of the heme- and Fe-DPIX-bound protein, to 444 and 430 nm, respectively.

Efforts to further enhance Fe-DPIX selectivity through mutations in or around pocket-1 were unsuccessful. Accord-

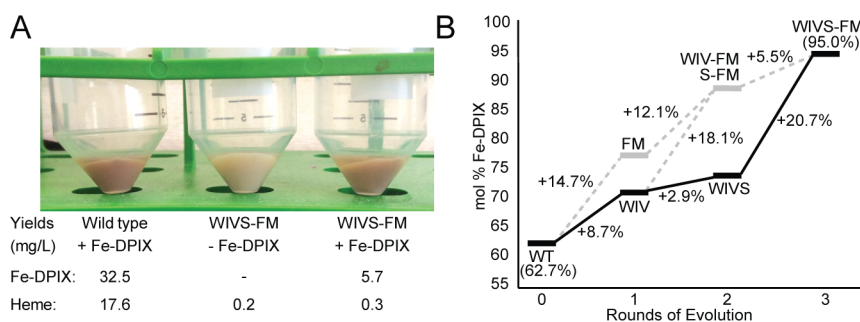


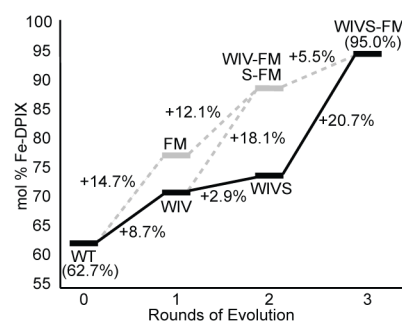
Figure 3. Selectivity of BM3h variants for Fe-DPIX. (A) Cell pellets of wild type BM3h and WIVS-FM after expressions in rich media in the presence or absence of Fe-DPIX. Red cell pellets are indicative of high levels of properly folded BM3h. Yields were determined by HPLC analysis. (B) Improvements in Fe-DPIX selectivity between variants along the original evolutionary trajectory (black bars and lines) and via alternative evolutionary paths (gray bars and dashed lines).

ingly, we focused subsequent libraries to pocket-2 using WIVS as a parent template. We again chose three residues—I153, G265, and F405 for randomization, each sampling the same 10 amino acids as our initial library. Screening 1000 transformants from this library yielded a single variant bearing two additional mutations G265F and F405M (WIVS-FM). Remarkably, this variant showed no detectable heme peak in the CO-bound absorbance spectrum under screening conditions (Figure 2B).

WIVS-FM Is Highly Selective for Fe-DPIX. To more thoroughly investigate cofactor selectivity, evolved BM3h variants were expressed in the presence of 10 μ M Fe-DPIX in either minimal media (low cellular heme concentrations) or rich media (TB, that is, in the presence of endogenous heme), and the Fe-DPIX and heme content of purified BM3h preparations was quantified via HPLC (Table 1, Figure S2). Minimal media expressions provided BM3h variants that were highly enriched (>98 mol %) for Fe-DPIX (Table 1 and Figure S3A), and the most selective variant, WIVS-FM, showed no detectable heme binding under these conditions. On the other hand, when expressed in rich media, wild type BM3h showed considerable contamination by native heme (Fe-DPIX/heme = 62.7 mol %:37.3 mol %; Figure 3A and B, Table 1 and Supporting Information Figures S2A and S3B).

Enhancements in Fe-DPIX selectivity as measured by Soret band absorbance (Figure 2B) were corroborated by HPLC quantitation. WIV and WIVS, which contain mutations isolated to pocket-1, showed small but iterative improvements in Fe-DPIX selectivity (71.4 mol % and 74.3 mol %, respectively; Figure 3B, Table 1 and Figures S2A and S3B). Selectivity was significantly improved in WIVS-FM, which in rich media provided protein purities comparable to those produced under conditions that restrict heme biosynthesis (Fe-DPIX/heme = 95.0 mol %:5.0 mol %; Figure 3A,B, Table 1, and Figures S2A and S3B). The ratio of cofactor-bound- to apo-WIVS-FM was found to be consistent with levels of heme incorporation in wild type BM3h (Figure S9). Furthermore, expression of WIVS-FM in rich media and in the absence of Fe-DPIX produced only small quantities of heme-bound WIVS-FM (<0.5 mg/L; Figure 3A), the majority of which possessed a CO-bound Soret peak at 420 nm, indicative of a misligated heme state (often called P420, Figure S4A).³⁵ These data suggest that WIVS-FM effectively restricts heme from the active site, while accommodating Fe-DPIX in an orthogonal fashion.

Mutations in Pocket-1 and Pocket-2 Provide Additive Improvements in Fe-DPIX Selectivity. While we pursued an evolutionary trajectory that initially targeted mutations to pocket-1 (followed by pocket-2 in later rounds), efforts to affect



changes in Fe-DPIX selectivity could feasibly use either cavity as a starting point. The most significant improvement in Fe-DPIX selectivity was achieved upon the addition of two mutations to pocket-2 (i.e., G265F and F405M in WIVS-FM). This observation led us to question whether improvements that result from these mutations were dependent on amino acid substitutions identified in prior rounds of selection, or whether pocket-2 mutations could function in isolation.

To examine the role of mutational directionality in orthogonal enzyme/cofactor pair evolution, we constructed three additional BM3h variants sampling alternative evolutionary trajectories (Figure 3B and Figure S4B). Variant BM3h-G265F/F405M (denoted FM), which contains only pocket-2 mutations, increased the mol % incorporation of Fe-DPIX to 77.4%, as compared to 62.7% in the wild type scaffold (Table 1). The degree of enrichment afforded by these two mutations alone (+14.7%) is similar in magnitude to that observed upon addition of the same mutations to WIVS (+20.7%) (Figure 3B). Grafting the G265F/F405M mutations onto the WIV scaffold (lacking the A406S mutation) to produce WIV-FM (BM3h-T269V/L272W/L322I/G265F/F405M) produced similar gains in Fe-DPIX selectivity (+18.1 mol %) (Figure 3B). These results show that pocket-1 and pocket-2 mutations, in isolation, are sufficient to provide significant improvements in Fe-DPIX binding and provide additive enhancements when combined. The functional independence of both pockets may permit the evolution of protein scaffolds that selectively recognize more complicated cofactor structures including heme analogues bearing asymmetric-substitution patterns in place of the vinyl moieties.

In contrast to other mutations, A406S showed greater context-dependent effects with respect to the parent scaffold. While the introduction of A406S into WIV (to produce WIVS) provided only a modest improvement in Fe-DPIX binding (2.9 mol %), this mutation provided a 12.1 mol % improvement in binding in the context of the FM scaffold (S-FM) (Figure 3B). While our library designs include this residue in pocket-1, it is situated on an active site helix that occupies a position at the interface of both cavities. These results suggest that mutations at A406 may facilitate pocket-2 remodeling in a manner independent of pocket-1.

Fe-DPIX Selectivity Increases as Result of Decreased Stability of the Heme-Bound Enzyme. Increased Fe-DPIX selectivity in BM3h variants may reflect improved enzyme/cofactor interactions with the Fe-DPIX scaffold, decreased affinity/stability with respect to native heme, or a combination of both. To investigate the extent to which these effects

contribute to observed increases in Fe-DPIX binding, we measured the stability of purified heme- and Fe-DPIX-bound variants (Table 1) as a function of T_{50} (the temperature at which half the protein remains folded after a 10 min incubation). Native BM3h/heme was more stable than BM3h/Fe-DPIX by ~ 5 °C ($T_{50, \text{heme}} = 55.5$ °C, $T_{50, \text{Fe-DPIX}} = 50.4$ °C; Table 1), consistent with the fact that the wild type pocket is highly optimized for heme. Mutations that confer increases in Fe-DPIX selectivity resulted in lower stability of the heme-bound protein. While significant decreases in stability relative to wild type were observed for heme-bound WIV ($T_{50, \text{heme}} = 52.7$ °C; Table 1) and WIVS ($T_{50, \text{heme}} = 49.7$ °C; Table 1), these variants maintained similar stabilities in the presence of Fe-DPIX ($T_{50, \text{Fe-DPIX}} \approx 50$ °C; Table 1). WIVS-FM/heme expressions resulted in a misfolded P420 state (Figure S4A), which prevented thermostability measurements. This result suggests that heme-bound WIVS-FM is further destabilized relative to other variants.

The decrease in stability observed in WIVS-FM/heme was accompanied by a slight loss in stability of WIVS-FM/Fe-DPIX ($T_{50, \text{Fe-DPIX}} = 47.1$ °C; Table 1). In attempt to improve the stability of the WIVS-FM/Fe-DPIX pair, we introduced two mutations (L52I and I366V, to produce WIVS-FM-IV), which have previously been shown to increase the thermostability of BM3h variants.³⁹ WIVS-FM-IV/Fe-DPIX showed increased yield and stability ($T_{50, \text{Fe-DPIX}} = 51.4$ °C; Table 1) compared to WIVS-FM/Fe-DPIX. However, these gains were accompanied by a concomitant increase in stability and yield of the heme-bound protein, resulting in a loss of Fe-DPIX selectivity (Table 1, Figures S3A,B, S4C). These stability trends suggest that engineered mutations provide enrichment in Fe-DPIX primarily through destabilization of the heme-bound protein.

Structural Determinants of Fe-DPIX Selectivity in Evolved BM3h Variants. To elucidate the molecular basis for Fe-DPIX selectivity, we determined the crystal structures of WIVS and WIVS-FM to 2.34 and 2.16 Å, respectively (see Table S4 for statistics on data collection and refinement). Each structure contains eight molecules in the unit cell. Overall, both structures closely resemble wild type BM3h (Figure S5), with the most significant changes occurring to side chain positions in the heme-binding pocket.^{36,37} WIVS and WIVS-FM aligned to the substrate-free structure of wild type BM3h³⁶ (PDB: 2IJ2, molecule A) with average rmsd values of 0.88 and 0.92 Å, respectively, and to the substrate-bound structure³⁷ (PDB: 1JPZ, molecule A) with rmsd values of 0.40 and 0.43 Å, respectively.

Active site mutations of WIVS-FM appear to fill the cavities imparted by deletion of the heme-vinyl groups. The indole side chain of L272W occupies the space previously filled by the vinyl group in pocket-1 (Figure 4A). The side chain of L322I, which packs against L272W, may orient the tryptophan side chain to more favorably exclude heme. The T269V mutation overlays closely with the isosteric wild type side chain, and while this mutation may not contribute significantly to steric occlusion of native heme, it may increase hydrophobicity in pocket-1. In addition, this mutation interrupts a cognate hydrogen bond between the backbone carbonyl of residue 265 with the T269 side chain (Figure S7A),³⁶ which may lead to observed backbone conformational changes in the I-helix, discussed below. The A406S mutation appears to improve packing with the porphyrin ring. In pocket-2, the G265F mutation fills the vinyl cavity of pocket-2 (similar to L272W in pocket-1) while

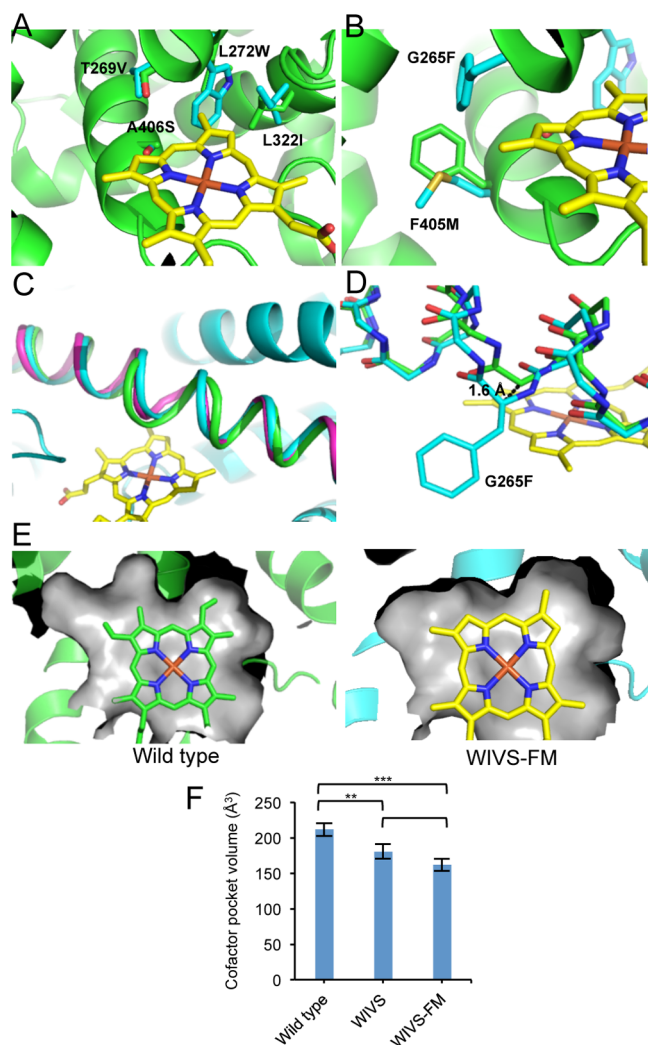


Figure 4. Molecular determinants of Fe-DPIX selectivity. (A) Pocket-1 and (B) pocket-2 of wild type BM3h (green, 2IJ2) overlaid against WIVS-FM side chains (cyan). The Fe-DPIX cofactor of WIVS-FM is shown in yellow. (C) Cartoon overlay of the I-helix of WIVS-FM (cyan) with that of substrate-free wild type BM3h (green, 2IJ2) and substrate-bound BM3h (purple, PDB: 1JPZ³⁷). (D) The I-helix of WIVS-FM (cyan) overlaid with the substrate-free wild type structure (green, 2IJ2), shown in stick representation. Only the side chain of residue G265F is shown for clarity. (E) The cofactor-binding pocket (gray surface) of the wild type enzyme (green, 2IJ2) compared to WIVS-FM (cyan, cofactor in yellow). (F) Quantified cavity volumes along the evolutionary trajectory. Error bars represent standard deviations. $n = 8$ molecules; (*) $p < 0.01$, (**) $p < 0.0001$, (***) $p < 0.0000001$.

F405M appears to create a flexible packing interface to accommodate the G265F mutation (Figure 4B).

Several unexpected features were observed in the crystal structures of both WIVS and WIVS-FM. For example, the conformation of the Fe-DPIX cofactor is rotated 180° about the plane of the porphyrin with respect to the preferred conformation typically observed in heme-bound BM3h (see heme/Fe-DPIX methyl groups in Figure 4E and Figure S6A,B,E). Modeling suggests that, in the “un-flipped” conformation, steric clashes would occur between the Fe-DPIX exocyclic-methyl groups and the side chains of A406S and G265F; however, these inhibitory interactions are alleviated in the ring-flipped conformation (Figure S6C,D). This alternate

“ring-flipped” porphyrin conformation is observed for heme in high resolution structures of BM3h and is estimated to make up less than 20% of the population in the wild type enzyme.³⁶ The ability of the cofactor to occupy different conformations may allow some variants to maintain heme binding by circumventing steric clashes between the heme vinyl moieties and the introduced amino acid mutations (e.g., clashes between the heme vinyl group in pocket-1 and the L272W side chain are avoided in the “ring-flipped” conformation) (Figure S6E).

The structures of WIVS and WIVS-FM also show unexpected rearrangements in the backbone conformation of the BM3h I-helix (a long, conserved helix that spans the length of the P450 active site and is important for catalysis). Substrate-free structures of wild type BM3h show a significant kink in the middle of the I-helix due to an interruption of the i–i+4 hydrogen bonding pattern by a conserved water molecule, which inserts itself between the carbonyl of I263 and the amide nitrogen of E267.³⁷ In substrate-bound structures, this water molecule is displaced resulting in a straightening of the I-helix.³⁷ In both WIVS and WIVS-FM, which were crystallized in the absence of substrate, we do not observe the typical water molecule between I263 and E267 and the I-helix adopts an unknicked helical backbone conformation that more closely resembles the substrate-bound form of the protein (Figure 4C and Figure S7A,B). Notably, the I-helix becomes progressively less distorted along the evolutionary trajectory.

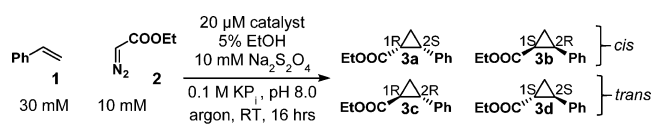
Previous structural studies of P450_{BM3} variants have noted that mutations in the I-helix can lock the enzyme in the substrate-bound conformation even in the absence of substrate.^{36,40,41} Unbending of the I-helix observed in WIVS may result from the T269V mutation, which interrupts a cognate backbone carbonyl-side chain hydrogen bond between G265 and the side chain of T269 (Figure S7A). Further straightening of the helix is observed in WIVS-FM with the addition of the G265F and F405M mutations (Figure S7A,C). Notably, G265F, resides in the I-helix; the removal of a helix-breaking glycine residue at this location may contribute significantly to increased helicity. As a result of this backbone conformational change, the C α atom of G265F (in WIVS-FM) shifts 1.6 Å with respect to the wild type structure (Figure 4D). This movement helps prevent steric clashes between the phenylalanine side chain and the Fe-DPIX porphyrin ring (Figure 4D). This observation suggests that while the I-helix is well situated to interact with native heme, backbone conformational rearrangements may be important to accommodate mutations that enrich for artificial porphyrin binding.

In general, we observed a significant decrease in the size of the cofactor binding pocket of engineered BM3h variants when compared to the wild type enzyme (Figure 4E and Figure S8A). To quantify these differences, we calculated changes in solvent-accessible pocket volume in the immediate vicinity of the cofactor (Figure 4F and Figure S8B). To provide a statistical analysis, we computed active site volumes in all eight monomers of the WIVS and WIVS-FM structures, as well as eight molecules of substrate-free wild type BM3h from the structures 2IJ2, 1BU7, 2HPD, and 2BMH.^{36,42–44} The cofactor binding pocket volume shrinks substantially along the evolutionary trajectory (wild type = 212 Å³, WIVS = 181 Å³, WIVS-FM = 161 Å³; Figure 4F), providing a complementary binding surface for Fe-DPIX at the exclusion of the larger heme porphyrin.

WIVS-FM/Fe-DPIX Catalyzes Non-natural Carbenoid-Mediated Olefin Cyclopropanation. A major goal of this

work is to enable the generation of new catalysts for reactions not found in nature. To demonstrate the potential for using orthogonal enzyme/heme pairs as catalytic scaffolds, we examined the activity of WIVS-FM/Fe-DPIX in non-natural carbenoid-mediated olefin cyclopropanation. Recent work has shown that heme enzymes can be engineered as highly active and selective catalysts for this reaction.^{45–48} In particular, the mutation T268A in BM3h has been shown to be highly activating toward cyclopropanation.⁴⁵ Therefore, we introduced the T268A mutation into the WIVS-FM scaffold. The addition of this mutation did not affect selective Fe-DPIX recognition (Table S3). We then tested the *in vitro* activity of WIVS-FM T268A/Fe-DPIX in the model cyclopropanation reaction between styrene and ethyl diazoacetate (Table 2 and Figure

Table 2. Activities and stereoselectivities of biocatalysts for the reaction of styrene with ethyl diazoacetate



catalyst	yield	TTN ^a	dr (cis:trans)	ee ^b cis [%]	ee ^c trans [%]
heme	7	35	16:84	0	-11
Fe-DPIX	5	23	13:87	3	-11
BM3h T268A/heme	57	284	1:99	-6	-97
BM3h T268A/heme aerobic	2	11	10:90	-15	-42
WIVS-FM T268A/Fe-DPIX	44	221	12:88	-51	-46
WIVS-FM T268A/Fe-DPIX aerobic	12	59	12:88	-33	-37

^aTTN = total turnover number. ^b(1R,2S) – (1S,2R). ^c(1R,2R) – (1S,2S). TTN and stereoselectivities determined by chiral GC analysis.

S10). WIVS-FM T268A/Fe-DPIX shows levels of cyclopropanation activity near that of BM3h T268A/heme, although the selectivity of the T268A variant is altered in the context of WIVS-FM compared to the wild type protein. The observed changes in selectivity may be a result of altered substrate binding conformations caused by the observed backbone changes in the I-helix (described above).

Orthogonal P450-FeDPIX scaffolds were inactive in native P450-mediated monooxygenation reactions (Figure S11). As such, engineered FeDPIX variants provide a new enzyme scaffold that is exclusively competent for non-natural cyclopropanation catalysis, without competition with native P450 chemistry. We hypothesize that the loss of monooxygenation catalysis results from significant structural rearrangements in the I-helix, which has been shown to play a pivotal role in proton transfer events that are necessary for the P450 catalytic cycle.³⁷

The observation that WIVS-FM is no longer active in monooxygenation reactions led us to also investigate cyclopropanation under aerobic conditions, which are typically inhibitory toward P450-mediated carbenoid insertion reactions. WIVS-FM T268A/Fe-DPIX maintained a greater proportion of its activity and selectivity under aerobic conditions when compared to BM3h T268A/heme, further illustrating the potential of this orthogonal system as a starting point toward generating novel biocatalysts. Notably, the activity of the

enzyme/cofactor pair correlates with the activity of the free cofactor. This allows for potential orthogonal cofactors to be screened for a desired reaction activity prior to engineering the protein for selective binding. In this way, orthogonal enzyme/heme pairs allow for optimization of new chemistry via “evolution” of both the cofactor and protein.

CONCLUSIONS

We report the design and evolution of an orthogonal cytochrome P450 scaffold that shows altered specificity toward a non-natural metallocofactor, Fe-DPIX. WIVS-FM was isolated after only three rounds of directed evolution, sampling ~2100 total transformants, suggesting that limited-diversity randomization of the heme-binding cavity can produce rapid enhancements in selectivity for non-natural cofactors. Structural investigations suggests that isolated mutations exclude native heme through iterative reduction in size of the cofactor binding cavity, providing selective recognition of the smaller deuteroporphyrin scaffold. While WIVS-FM/Fe-DPIX no longer catalyzes native P450 monooxygenation reactions, it shows significant activity in non-natural cyclopropanation reactions, providing a new starting point for the development of non-natural biocatalysts.

We anticipate that this approach can be expanded to a range of synthetic porphyrin and nonporphyrin systems bearing alternate functionality that enables discrimination from native-heme and in parallel that tune the electronic properties of the metal center. In cases where the cofactor structure is significantly divergent from native heme, the scope of promiscuous transport by ChuA will need to be addressed. Evolution of ChuA prior to, or in parallel with, evolution of the orthogonal enzyme may be required for more complex scaffolds. Additionally, the very small levels of heme contamination observed for orthogonal enzyme preparations in rich media may complicate screens for novel catalytic activity, as care will have to be taken to ensure observed activity is not due to contaminating heme enzyme. However, this may not be an issue in screening for reactions that heme itself cannot catalyze.

This work provides a strategy for reshaping heme-binding pockets to recognize designed, artificial metallocofactors. For example, the ability of evolved Fe-DPIX-binding proteins to produce noniron proteins is currently being investigated. As was recently shown, alternative metal centers have the potential to greatly expand the reaction scope of heme enzymes⁴⁹ and thus is a promising direction for the generation of highly active orthogonal enzyme/heme pairs in reactions that cannot be catalyzed by native heme. In addition, the design of a panel of orthogonal proteins that selectively recognize unique cofactor scaffolds will allow for the expression of tailored metal-substituted proteins in cells. These engineered metalloproteins may then be integrated into biosynthetic pathways or used as probes of protein function. Accordingly, orthogonal enzyme/cofactor pairs represent versatile tools to expand nature's chemical repertoire.

ASSOCIATED CONTENT

Supporting Information

The Supporting Information is available free of charge on the ACS Publications website at DOI: 10.1021/jacs.6b05847.

Materials and methods including procedures for plasmid and library construction, protein expression and

purification, HPLC assays, library screening, carbon monoxide binding assays, thermostability measurements, extinction coefficient determination, protein crystallography, cavity volume calculations, and cyclopropanation reactions (PDF)

AUTHOR INFORMATION

Corresponding Author

*brustad@email.unc.edu

Notes

The authors declare no competing financial interest.

ACKNOWLEDGMENTS

We thank Dr. Frances Arnold (Cal Tech) and Dr. Alan Jasanoff (MIT) for providing plasmids pCWori-BM3h and pChuA, respectively, Dr. Mike Miley and the Redinbo lab (UNC-Chapel Hill) for help with crystallography experiments and Dr. Kathryn Matera (Elon) for helpful discussions. This work was supported by a DARPA Young Faculty Award (D13AP00024) and NSF Career Award (CHE-1552718) to E.M.B. E.W.R. was supported by an NSF Graduate Research Fellowship (DGE1144081).

REFERENCES

- (1) Hoffman, B. M.; Petering, D. H. *Proc. Natl. Acad. Sci. U. S. A.* **1970**, *67*, 637–643.
- (2) Wang, N.; Zhao, X.; Lu, Y. *J. Am. Chem. Soc.* **2005**, *127*, 16541–16547.
- (3) Fruk, L.; Kuo, C.-H.; Torres, E.; Niemeyer, C. M. *Angew. Chem., Int. Ed.* **2009**, *48*, 1550–1574.
- (4) Winter, M. B.; McLaurin, E. J.; Reece, S. Y.; Olea, C.; Nocera, D. G.; Marletta, M. a. *J. Am. Chem. Soc.* **2010**, *132*, 5582–5583.
- (5) Lelyveld, V. S.; Brustad, E.; Arnold, F. H.; Jasanoff, A. *J. Am. Chem. Soc.* **2011**, *133*, 649–651.
- (6) Winter, M. B.; Klemm, P. J.; Phillips-Piro, C. M.; Raymond, K. N.; Marletta, M. a. *Inorg. Chem.* **2013**, *52*, 2277–2279.
- (7) Heinisch, T.; Ward, T. R. *Curr. Opin. Chem. Biol.* **2010**, *14*, 184–199.
- (8) Petrik, I. D.; Liu, J.; Lu, Y. *Curr. Opin. Chem. Biol.* **2014**, *19C*, 67–75.
- (9) Pàmies, O.; Diéguez, M.; Bäckvall, J.-E. *Adv. Synth. Catal.* **2015**, *357*, 1567–1586.
- (10) Wilson, M.; Whitesides, G. *J. Am. Chem. Soc.* **1978**, *100*, 306–307.
- (11) Hyster, T. K.; Knörr, L.; Ward, T. R.; Rovis, T. *Science* **2012**, *338*, 500–503.
- (12) Srivastava, P.; Yang, H.; Ellis-Guardiola, K.; Lewis, J. C. *Nat. Commun.* **2015**, *6*, 7789.
- (13) Ohashi, M.; Koshiyama, T.; Ueno, T.; Yanase, M.; Fujii, H.; Watanabe, Y. *Angew. Chem., Int. Ed.* **2003**, *42*, 1005–1008.
- (14) Carey, J. R.; Ma, S. K.; Pfister, T. D.; Garner, D. K.; Kim, H. K.; Abramite, J. a.; Wang, Z.; Guo, Z.; Lu, Y. *J. Am. Chem. Soc.* **2004**, *126*, 10812–10813.
- (15) Kawakami, N.; Shoji, O.; Watanabe, Y. *ChemBioChem* **2012**, *13*, 2045–2047.
- (16) Brustad, E. M.; Arnold, F. H. *Curr. Opin. Chem. Biol.* **2011**, *15*, 201–210.
- (17) Heinisch, T.; Pellizzoni, M.; Dürrenberger, M.; Tinberg, C. E.; Köhler, V.; Klehr, J.; Häussinger, D.; Baker, D.; Ward, T. R. *J. Am. Chem. Soc.* **2015**, *137*, 10414–10419.
- (18) Hyster, T. K.; Ward, T. R. *Angew. Chem., Int. Ed.* **2016**, *55*, 2–16.
- (19) Bordeaux, M.; Singh, R.; Fasan, R. *Bioorg. Med. Chem.* **2014**, *22*, 5697–5704.
- (20) Woodward, J. J.; Martin, N. I.; Marletta, M. A. *Nat. Methods* **2007**, *4*, 43–45.

- (21) Nierth, A.; Marletta, M. a. *Angew. Chem., Int. Ed.* **2014**, *53*, 2611–2614.
- (22) Ji, D.; Wang, L.; Hou, S.; Liu, W.; Wang, J.; Wang, Q.; Zhao, Z. *K. J. Am. Chem. Soc.* **2011**, *133*, 20857–20862.
- (23) Carter-O'Connell, I.; Cohen, M. S. *Curr. Protoc Chem. Biol.* **2015**, *7*, 121–139.
- (24) Islam, K.; Chen, Y.; Wu, H.; Bothwell, I. R.; Blum, G. J.; Zeng, H.; Dong, A.; Zheng, W.; Min, J.; Deng, H.; Luo, M. *Proc. Natl. Acad. Sci. U. S. A.* **2013**, *110*, 16778–16783.
- (25) Whitehouse, C. J. C.; Bell, S. G.; Wong, L.-L. *Chem. Soc. Rev.* **2012**, *41*, 1218–1260.
- (26) Tracewell, C. A.; Arnold, F. H. *Curr. Opin. Chem. Biol.* **2009**, *13*, 3–9.
- (27) Fasan, R.; Meharena, Y. T.; Snow, C. D.; Poulos, T. L.; Arnold, F. H. *J. Mol. Biol.* **2008**, *383*, 1069–1080.
- (28) Salazar, O.; Cirino, P. C.; Arnold, F. H. *ChemBioChem* **2003**, *4*, 891–893.
- (29) Wong, T. S.; Arnold, F. H.; Schwaneberg, U. *Biotechnol. Bioeng.* **2004**, *85*, 351–358.
- (30) Modi, S.; Primrose, W. U.; Lian, L.; Roberts, G. C. K. *Biochem. J.* **1995**, *310*, 939–943.
- (31) Davydov, D. R.; Ponomarev, G. V.; Bobrovnikova-Marjon, E.; Haines, D. C.; Peterson, J. A. *Biotechnol. Appl. Biochem.* **2013**, *60*, 41–51.
- (32) Lopez, M. S.; Kliegman, J. I.; Shokat, K. M. *The Logic and Design of Analog-Sensitive Kinases and Their Small Molecule Inhibitors*; 1st ed.; Elsevier Inc., 2014; Vol. 548.
- (33) Baud, M. G. J.; Lin-shiao, E.; Cardote, T.; Tallant, C.; Pschibul, A.; Chan, K.; Zengerle, M.; Garcia, J. R.; Kwan, T. T.; Ferguson, F. M.; Ciulli, A. *Science* **2014**, *346*, 638–641.
- (34) Fischle, W.; Schwarzer, D. *ACS Chem. Biol.* **2016**, *11*, 689–705.
- (35) Guengerich, F. P.; Martin, M. V.; Sohl, C. D.; Cheng, Q. *Nat. Protoc.* **2009**, *4*, 1245–1251.
- (36) Girvan, H. M.; Seward, H. E.; Toogood, H. S.; Cheesman, M. R.; Leys, D.; Munro, A. W. *J. Biol. Chem.* **2007**, *282*, 564–572.
- (37) Haines, D. C.; Tomchick, D. R.; Machius, M.; Peterson, J. A. *Biochemistry* **2001**, *40*, 13456–13465.
- (38) Reetz, M. T. *J. Am. Chem. Soc.* **2013**, *135*, 12480–12496.
- (39) Fasan, R.; Chen, M. M.; Crook, N. C.; Arnold, F. H. *Angew. Chem., Int. Ed.* **2007**, *46*, 8414–8418.
- (40) Girvan, H. M.; Toogood, H. S.; Littleford, R. E.; Seward, H. E.; Smith, W. E.; Ekanem, I. S.; Leys, D.; Cheesman, M. R.; Munro, A. W. *Biochem. J.* **2009**, *417*, 65–76.
- (41) Girvan, H. M.; Marshall, K. R.; Lawson, R. J.; Leys, D.; Joyce, M. G.; Clarkson, J.; Smith, W. E.; Cheesman, M. R.; Munro, A. W. *J. Biol. Chem.* **2004**, *279*, 23274–23286.
- (42) Sevioukova, I. F.; Li, H.; Zhang, H.; Peterson, J. a; Poulos, T. L. *Proc. Natl. Acad. Sci. U. S. A.* **1999**, *96*, 1863–1868.
- (43) Ravichandran, K. G.; Boddupalli, S. S.; Hasermann, C. A.; Peterson, J. A.; Deisenhofer, J. *Science* **1993**, *261*, 731–736.
- (44) Li, H.; Poulos, T. L. *Acta Crystallogr., Sect. D: Biol. Crystallogr.* **1995**, *51*, 21–32.
- (45) Coelho, P. S.; Brustad, E. M.; Kannan, A.; Arnold, F. H. *Science* **2013**, *339*, 307–310.
- (46) Coelho, P. S.; Wang, Z. J.; Ener, M. E.; Baril, S. a; Kannan, A.; Arnold, F. H.; Brustad, E. M. *Nat. Chem. Biol.* **2013**, *9*, 485–487.
- (47) Gober, J. G.; Rydeen, A. E.; Gibson-O'Grady, E. J.; Leuthaeuser, J. B.; Fetrow, J. S.; Brustad, E. M. *ChemBioChem* **2015**, *17*, 394–397.
- (48) Bordeaux, M.; Tyagi, V.; Fasan, R. *Angew. Chem., Int. Ed.* **2015**, *54*, 1744–1748.
- (49) Key, H. M.; Dydio, P.; Clark, D. S.; Hartwig, J. F. *Nature* **2016**, *534*, 534.